Approaches for novel enzyme discovery from marine environments

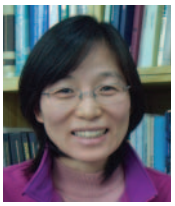

Hyun Suk Lee
Marine Biotechnology Research Department
•
leeh522@kordi.re.kr

The enormous pool of biodiversity in marine ecosystems is an excellent natural reservoir for acquiring an inventory of enzymes with potential for biotechnological applications. Moreover, the opportunity for sustainable resource management has been greatly enhanced by recent advances in culturing methods for recalcitrant microbes. The attention being given to marine genomic and metagenomic research has been increasing substantially in recent years, resulting in an exponential increase in the number of sequenced marine microbial genomes and completed metagenomic surveys. Screening genome database for genes that might encode new enzymes with interesting properties can potentially provide a shortcut in the development process for commercial enzymes.

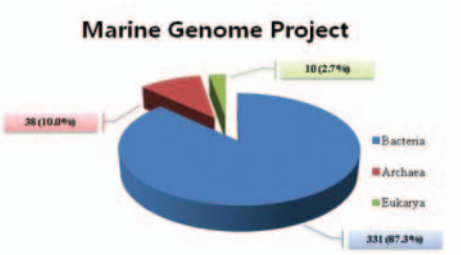

[Figure 1]
Marine genome projects performed until January in 2009. Based on the information by Genomes OnLine (http://www.ncbi.nlm.nih.gov/Genbank/index.html).

Enzyme	Source	Screening method
Esterases	Deep-sea sediment	Functional
	Deep hypersaline basin	Functional
	Arctic sediment	Functional
	surface seawater	Functional
Lipases	Tidal flat sediment	Functional
	Deep-sea sediment	Functional
	Marine sediment	Functional
β-Lactamases	Cold-seep sediments	PCR
Chitinases	Sargasso Sea	PCR
	Bay estuary	Functional
Amidases	Marine sediments	Functional
Cellulase	Sargasso Sea	Sequencing
Alkane hydroxylase	Deep-sea sediment	Sequencing
Proteases	Antarctic sea water	Sequencing

[Table 1]
Metagenomic screening of enzymatic activities from marine environmental samples.

mplicit formulation with the boundary element method for nonlinear radiation of water waves

Hong Gun Sung
Marine Structure & Plant Research Department
•
hgsung@moeri.re.kr

An accurate and efficient numerical method is presented for two-dimensional nonlinear radiation problem of water waves. The wave motion that occurs on water due to an oscillating body is described under the assumption of ideal fluid flow. The governing Laplace equation is effectively solved by utilizing the GMRES (Generalized Minimal RESidual) algorithm for the boundary element method (BEM) with quadratic approximation. The intersection or corner singularity in the mixed Dirichlet-Neumann problem is resolved by introducing discontinuous elements. The fully implicit trapezoidal rule is used to update solutions at new time-steps, by considering stability and accuracy. Traveling waves generated by the oscillating body are absorbed downstream by the damping zone technique. To avoid the numerical instability caused by the local gathering of grid points, the re-gridding technique is employed, so that all the grids on the free surface may be re-distributed with an equal distance between them. Nonlinear radiation force is evaluated by means of the acceleration potential. For a mixed Dirichlet-Neumann problem in a computational domain with a wavy top boundary, the present BEM yields numerical solutions for the quadratic rate of convergence with respect to the number of boundary elements. It is demonstrated that the present time-marching and radiation condition work successfully for nonlinear radiation problems of water waves. The results concur reasonably well with other numerical computations.

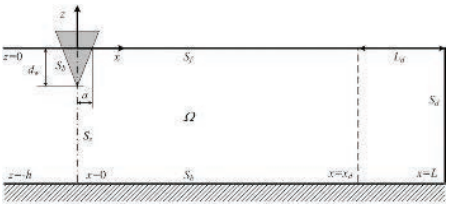

[Figure 1]
Coordinate system and definition sketch of the present wave-body interaction problem

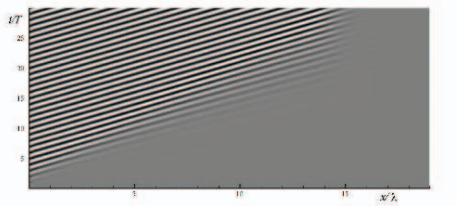

[Figure 2]
Contour plot for the free surface shape (A_w/a=0.6and ω^2 a/g =0.2)

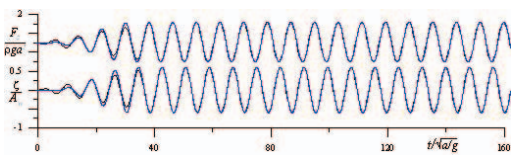

[Figure 3]
Vertical displacement of the body (lower two lines) and the nonlinear radiation force (upper two lines) (Black lines; Tanizawa & Clement, 2000, Blue lines; Present; A_w/a=0.6and ω^2 a/g=0.6)

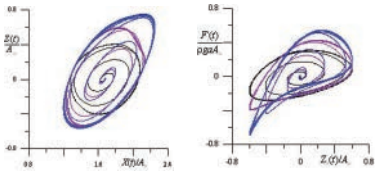

[Figure 4]
Trajectories of the far upstream point, the nonlinear radiation force vs. the body motion for (black line: ω^2 a/g=0.4,violet line: ω^2 a/g =0.8, blue line:=ω^2 a/g 1.2and A_w/a=0.6 for all cases)

The 20 January 2007 ML 4.8 Odaesan earthquake and its implications for regional tectonics in Korea

Kwang-Hee Kim
Ocean Satellite Remote Sensing & Observation Technology Research Department
•
kwanghee@kordi.re.kr

A moderate-sized earthquake (ML 4.8) occurred in the mid-east Korea Peninsula on 20 January 2007. It was the largest inland earthquake to occur there since the inception of a modern seismic observation system. Although only four aftershocks were noticed in previous studies, a careful review of continuous data revealed that the main event was accompanied by at least 74 micro foreshocks and aftershocks. A subset of 25 events was selected for further analysis to determine precise earthquake locations, focal mechanism solutions, and the current status of regional tectonic stress, as well as to answer questions raised about the sequence. Earthquake hypocenters were seen to be more clustered after the HypoDD relocation. A source radius of 1 km for the main event was estimated based on the distribution of precisely determined aftershock locations. Focal mechanism solutions of larger events in the sequence suggest either a left-lateral strike-slip fault trending WNW-ESE or a right-lateral strike slip fault trending NEN-SWS as the responsible structure. Although the Woljeongsa Fault striking NEN-SWS in the local geological map matches one of the proposed trends, precise earthquake relocation results gave a contradictory result, showing that a previously unknown WNW-ESE striking fault was responsible for the earthquake sequence. We also observed an unusual lack of large-magnitude aftershocks, a relatively large stress drop during the main event, and no previous earthquake record in the region. Observations made in the study consistently indicate the sequence nucleated along a less-developed fault. Focal mechanism solutions suggest the current status of tectonic stress governing earthquake generation in Korea is ENE-WSW compression and NNW-SSE extension.

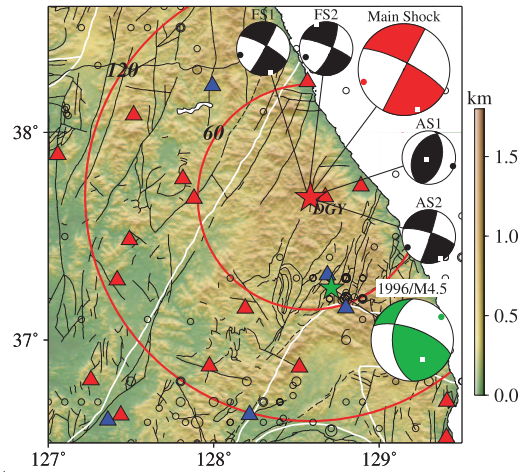

Fault locations in the study area from the geological map of Korea (KIGAM, 2002) are shown in black lines. The star and beach ball plot in red show the hypocenter and focal mechanism solution of the main event. Focal mechanism solutions of two foreshocks (FS1 and FS2) and two aftershocks (AS1 and AS2) are shown in black. Seismic station DGY is the closest station to the main event and marked on the figure. It also shows the location and focal mechanism solution for the 1996 ML4.5 Yeongwol earthquake. Red circles are 60 km and 120 km equidistant, respectively, from the Odaesan earthquake epicenter. Tectonic boundaries are shown as white lines.

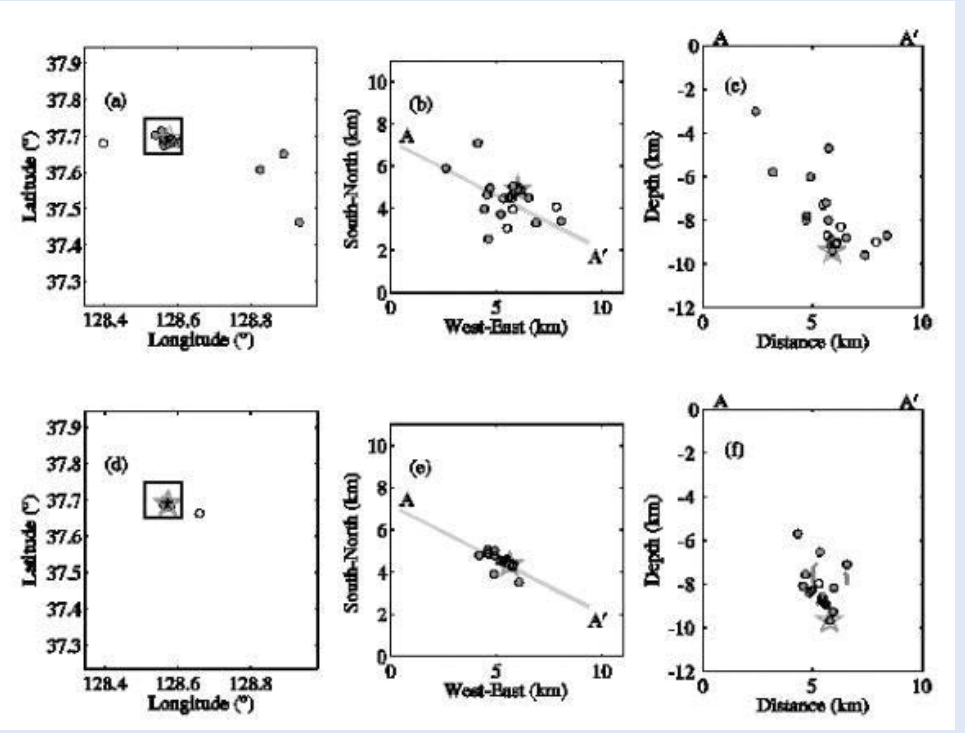

Earthquake relocation of the Odaesan earthquake sequence using HypoDD. A subset of twenty-four events recorded by more than 4 seismic stations was selected for initial earthquake location and relocation. (a) Map view of initial earthquake locations. The mainshock, foreshocks, and aftershocks are presented as a star, open circles, and closed circles, respectively. Most earthquakes in the sequence are clustered in a small region marked by a square, which is the area of (b). (b) Map view of initial earthquake locations marked by a square in (a). (c) Cross-sectional view of the initial earthquake hypocenters along A-A′ in (b). Note, both map and cross-sectional views of initial earthquake hypocenters do not show any clear seismicity pattern. (d) Map view of earthquake epicenters relocated by HypoDD. (e) Relocated earthquake hypocenters in the square marked in (d). A linear seismicity striking WNW-ESE is clear. (f) Cross-sectional view of relocated earthquake hypocenters along A-A′. Note foreshocks are clustered in a very small region. Estimated source rupture area determined by aftershock distributions is shown by a gray circle.

Prochaetosoma dokdoense sp. nov. (Nematoda: Draconematidae) from Dokdo, Korea: First record of the genus Prochaetosoma from a shallow subtidal zone in the northwest Pacific Ocean

Rho, Hyun Soo
Dokdo Research Center
•
hsrho@kordi.re.kr

A draconematid nematode Prochaetosoma dokdoense sp. nov., first discovered in December 2006 at a subtidal zone of Dokdo, Korea, the northwest Pacific Ocean, is described. This new species was obtained from coarse detritus and shell gravels. Prochaetosoma dokdoense sp. nov. differs from all the species hitherto described by the following combination of characteristics: longer slender body (910-1175 ß≠), elongate loop-shaped amphidial fovea in male (distal end of ventral arm slightly curved anteriorly), eight cephalic adhesion tubes in both sexes positioned just anterior to swollen pharyngeal region, number of posterior sublateral adhesion tubes (6 in male and 6-10 in female) and posterior subventral adhesion tubes (7-8 in male and 8-9 in female), longer spicule length (78-86 ß≠), long cylindro-conoid tail (114-131 ß≠ in male and 116-131 ß≠ in female) and higher ratio c°« (6.5-7.5 in male and 7.4-9 in female). A table comparing the major differential diagnostic characteristics of the species of the genus Prochaetosoma Micoletzky, 1922 is presented. For a reliable understanding of the geographic distribution and species identification of the genus Prochaetosoma, a pictorial key showing the relative length of non-annulated tail terminus to total tail length in both sexes is included, together with a dichotomous species identification key based on adults and fourth-stage juvenile as far as known. This is the first record of the genus Prochaetosoma in the northwest Pacific Ocean.

[Figure 1]
DIC photomicrograph of *Prochaetosoma dokdoense* sp. nov, female.

[Figure 2]
Prochaetosoma dokdoense sp. nov., female, allotype

F???

Young Gyu Park
Climate Change & Coastal Disaster Research Department/
•
ypark@kordi.re.kr

Using high resolution model results and the trajectories of ARGO floats, we report direct flows from the Ulleung Basin into the Yamato Basin through a gap between the Oki Spur and the Yamato Rise over the southern part of the East/Japan Sea. The gap is subdivided into two narrow (northern and southern) passages by a seamount located in the middle. The flows, therefore, are narrow and this explains why this flow was not reported earlier. More than half of the 25 ARGO floats, which operated around the gap, drifted through the gap or area near it. The strength of the throughflow estimated using the trajectories of the floats at parking depth is comparable to the mean deep flow found over the southwestern part of the East/Japan Sea. A high resolution regional ocean model whose overall circulation pattern over the Ulleung Basin is consistent with those from previous studies shows that the flow through the gap is supplied mainly by eastward flows crossing the mouth of the basin, and secondarily by the cyclonic circulation following the outer perimeter of the basin. Thus the throughflow is an important component of the deep circulation over the southern East/Japan Sea, and the narrow gap, where the flow is well confined, would be a good place to study the deep circulation.

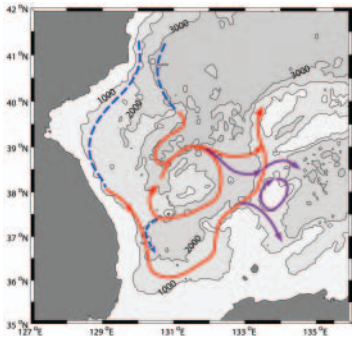

[Figure 1]
A schematic of flow patterns over the southwestern part of East/Japan Sea. The purple parts are based on results from the current study. The remaining parts are from Fig. 4 of Park et al. (2004).

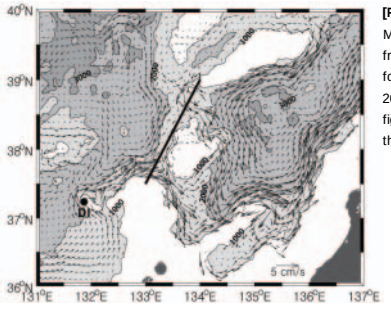

[Figure 2]
Mean circulation pattern at 700 m from average of the model results for the period between 1993 and 2002. Across the line shown in the figure the volume flux of the throughflow in Fig. 3 is estimated.

[Figure 3]
Climatological monthly mean volume fluxes of the throughflow across the line in Fig. 2 between top and bottom (dashed line) and below 200 m (solid line).

Changes in gene expression profile of medaka fish with acute toxicity of Arochlor 1260, a Polychlorinated Biphenyl mixture

Seung shic Yum
South Sea Environment Research Department
•
syum@kordi.re.kr

Differential gene expression profiling was performed with a cDNA microarray in the liver tissue of the medaka fish, Oryzias latipes, after exposure to Arochlor 1260, a polychlorinated biphenyl (PCB) mixture, which is used as a coolant and insulating fluid for transformers and capacitors and is classified as a persistent organic pollutant. Twenty-six differentially expressed candidate genes were identified. The expression of 12 genes was up-regulated and that of 14 genes was down-regulated. These genes are associated with the cytoskeleton, development, endocrine/reproduction, immunity, metabolism, nucleic acid/protein binding, and signal transduction, or were uncategorized. The transcription of molecular biomarkers known to be involved in endocrine disruption (e.g., vitellogenins, choriogenins, and estrogen receptor α) was highly up-regulated. The same tendencies in gene expression changes were observed with real-time quantitative PCR (qRT-PCR) analysis, which was conducted to examine 12 selected candidate genes. These genes could be used as molecular biomarkers for biological responses to toxic chemicals, especially endocrine disrupting and carcinogenic chemicals contamination in aquatic environments.

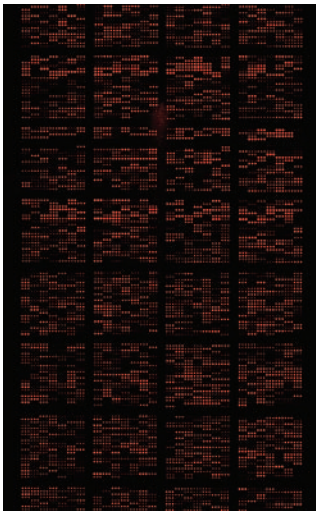

[Figure 1]
cDNA hybridization to microarray.

[Table 3]
Quantification by real-time quantitative PCR of the changes in the expressions of the 12 selected genes. The microarry results are shown in parallel.

Gene	Fold difference	
	qRT-PCR	Microarray
Estrogen receptor α	6.39	7.21
Vitellogenin 1 (ol-vit1)	586.10	377.62
Choriogenin H minor	18.70	17.93
Choriogenin L	13.88	5.20
Cytokeratin 17	36.89	3.84
Annexin max3 (anxa1)	1.70	2.29
Kallikrein precursor	-7.14	-2.70
Complement component C4 (c4)	-5.26	-2.78
Wap65	-5.00	-2.04
Cytochrome P450 2D	-5.00	-2.78
Hepatic lipase (lipc)	-3.70	-2.13
TRAP γ-chain (ssrg)	-5.00	-2.17

[Table 1]

Induction and repression of gene expression after Arochlor 1260 exposure in O. latipes, obtained with microarray analysis. The numbers indicate significant differences in the fold induction or repression relative to the expression in the control group ($P < 0.01$).

Category	Gene	FD*	Accession No.
Cytoskeleton	Cytokeratin 17	3.84	Z19574.1
	Type I cytokeratin, enveloping layer	2.74	BC065653.1
	Beta actin (ACT1)	2.48	AF043384
Development	HOXC5A	-1.89	AB026960
Immune	MHC Class I A	-1.96	AB026977
	T-cell acute lymphoblastic leukemia associated antigen 1	-2.17	AU178455
	Complement component C4	-2.78	AB025577
Metabolism	Paraoxonase 1	2.01	BC091403.1
	Malate dehydrogenase A (MdhA)	-1.89	AY161292
	Cytochorome P450 2N2	-2.04	AU179480
	Cytochrome P450 2N1	-2.22	BM280439
	Cytochrome P450 2J5	-2.27	AV669103
	Cytochrome P450 2D	-2.78	AU180871
	Hepatic lipase	-2.13	BM187526
Nuc./Prot. binding	Heat shock protein 70	-2.00	D13669.1
	Warm-temperatire-acclimation-related-65 kDA protein	-2.04	AB075198
	Translocon-associated protein γ-chain	-2.17	AV669630
Endocrine/Reproduction	Vitellogenin 1	377.62	AB064320
	Vitellogenin A2 precursor	109.82	AU180054.1
	Choriogenin H minor	17.93	AB025967
	Estrogen receptor α	7.21	AB033491
	Choriogenin L	5.20	AF500194
	Choriogenin H	2.70	D89609
Signal transduction	Annexin max3	2.29	Y11254
	Membrane guanylyl cyclase 4	1.95	AB000900
Non- categorized	Plasma kallikrein precursor	-2.70	AU179805

***FD: Fold difference**

[Table 2]

List of real-time quantitative PCR primers used to amplify the selected genes and the α-*tubulin* gene of *O. latipes*.

Gene	Nucleotide sequence	Gene	Nucleotide sequence
Vitellogenin 1(ol-vit1)	Forward 5′ -AATGGACGCTTGGCCAGAAA-3′	*Hepatic lipase (lipc)*	Forward 5′ -CCACATGTTCCTCCACACAG-3′
	Reverse 5′ -GCAACTGCAGGCAAGGTGAG-3′		Reverse 5′ -ATCAAGAAGGTTCGCACAGG-3′
Choriogenin H minor	Forward 5′ -GATGCTGACTACCCTGTCAC-3′	*TRAP r-chain (ssrg)*	Forward 5′ -GAAACGCTCTCATCGTCTCC-3′
	Reverse 5′ -GCTAGGGTCAGATGGAGAAG-3′		Reverse 5′ -TAGCCTCGTAGTCCGCTACC-3′
Choriogenin L	Forward 5′ -AAGGAGGTCAGTGGAGCAGA-3′	*Kallikrein precursor*	Forward 5′ -TCAGACAGCCTGTCAGAACA-3′
	Reverse 5′ -CCTTCCCATTCCAGAACTGA-3′		Reverse 5′ -CTGACACTGGTCTGCATTATC-3′
Estrogen receptor α	Forward 5′ - GAGGCAAGATCAAACCTGAG-3′	*Complement*	Forward 5′ -GAAGGAGAACTCTGTCCGAG-3
	Reverse 5′ - AGGTGCAGTCAGTCAACTTG-3′	*component C4 (c4)*	Reverse 5′ -CTGGCATGTTAGCTGATTGG-3′
Cytokeratin 17	Forward 5′ - TGGTCTTGGTTCTGGTGGTT-3′	Cytochrome P450 2D	Forward 5′ -CGCTGCTTCTTCCATTTCTC-3
	Reverse 5′ - CATTGAGGTTCTGCATGGTG-3′		Reverse 5′ -CCACAGTTGGCTGAAACGTA-3′
Annexin max3(anxa1)	Forward 5′ -CTGGATGACACTAAAGGAGAC-3′	α -tubulin	Forward 5′ -AAGGCATACCACGAGCAGTT-3
	Reverse 5′ -TGCACGTGATCTGAATGCAC-3′		Reverse 5′ -TTGCTAAGCATGCAGACAGC-3′
Wap65	Forward 5′ -CGATGCTGCATTTGTCTGCC-3′		
	Reverse 5′ -CCGTGCATTCAGTCCTGTCA-3′		

Inhibitory effect of diphlorethohydroxycarmalol on melanogenesis and its protective effect against UV-B radiation-induced cell damage

Heo, Soo-Jin
Marine Living Resources Research Department
•
sjheo@kordi.re.kr

In this study, potential inhibitory effect of 21 species of marine algae on melanogenesis was assessed via tyrosinase inhibitory effect. The Ishige okamurae extract tested herein evidenced profound tyrosinase inhibitory effect, compared to that exhibited by other marine algae extracts. Thus, I. okamurae was selected for use in further experiments, and was partitioned with different organic solvents. Profound tyrosinase inhibitory effect was detected in the ethyl acetate fraction, and the active compound was identified as the carmalol derivative, diphlorethohydroxycarmalol (DPHC), which evidenced higher levels of activity than that of commercial whitening agent. Intracellular reactive oxygen species (ROS) induced by ultraviolet (UV)-B radiation was reduced by the addition of DPHC and cell viability was dose-dependently increased. Moreover, DPHC demonstrated strong protective properties against UV-B radiation via damaged DNA tail length and morphological changes in fibroblast. Hence, these results indicate that DPHC isolated from I. okamurae has potential whitening effects and prominent protective effects on UV-B radiation-induced cell damages which might be used in pharmaceutical and cosmeceutical industries.

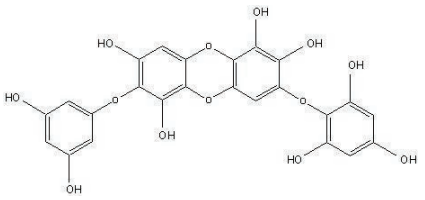

[Figure 1]
Chemical structure of diphlorethohydroxycarmalol (DPHC)

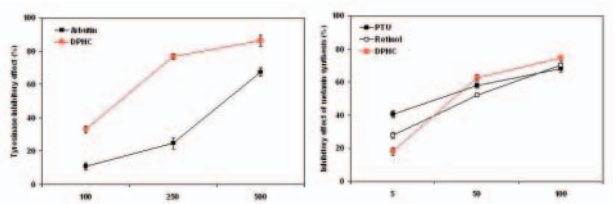

[Figure 2]
Inhibitory effect of DPHC on tyrosinase (left) and melanin synthesis (right)

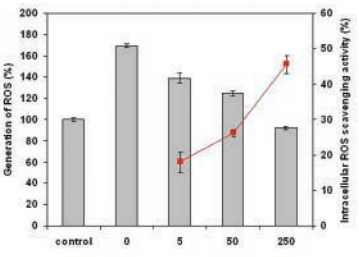

[Figure 3]
Protective effect of DPHC on UV-B radiation-induced cell damage

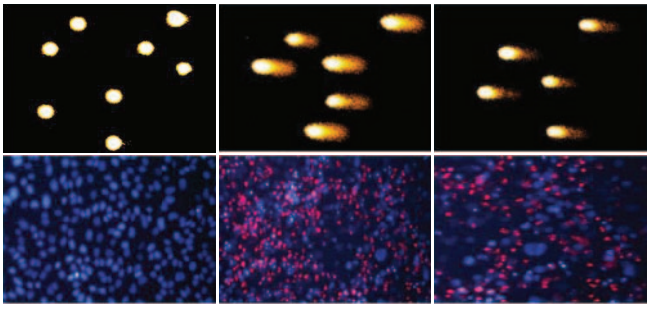

[Figure 4]
Photomicrographs of DNA damage and migration observed under DPHC

Phytoplankton viability in ballast water from international commercial ships berthed at ports in Korea

Jung-Hoon Kang
South Sea Environment Research Department
•
jhkang@kordi.re.kr

Despite the increasing recognition of risks of marine invasion, viability of phytoplankton transferred via ballast water with foreign port sources has previously not been studied in Korea. Thus, we investigated the viability of phytoplankton from ballast water of international commercial ships berthed at the ports of Ulsan and Onsan, Korea. The incubation conditions used were temperatures of 13°ΔC to represent ambient water and 20°ΔC to represent the thermal optimum, as well as nutrients in ballast water, shipside water, and F/2 medium. Phytoplankton in new (~7 days) and old (20 and 23 days) ballast water survived when incubated under the nutrients typical of shipside water and F/2 medium at 13°ΔC and 20°ΔC. Colonization process was mostly dominated by Skeletonema costatum, Cylindrotheca closterium and pennate diatoms (<10 •Ïm in diameter). S. costatum and C. closterium were persistent during incubation time, whereas pennate diatoms dominated in the three types of media from doubling to last phase of growth. This study showed that bloom-forming and pennate diatoms appear to be the species most likely to become successfully established in the two ports.

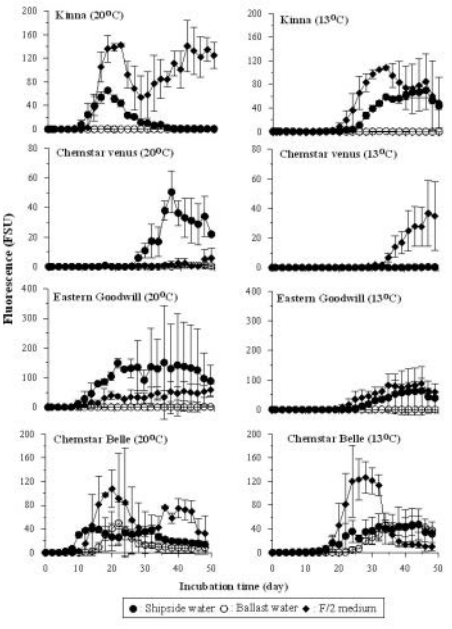

[Figure 1]
Temporal variations in growth of phytoplankton cultured in ballast water, shipside water, and F/2 medium at 13°C and 20°C in January 2006.

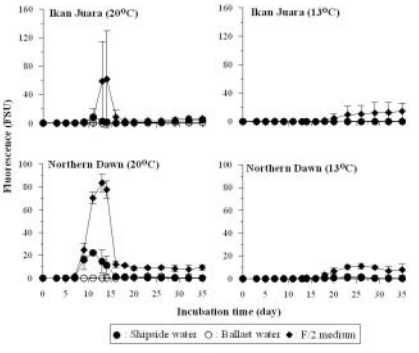

[Figure 2]
Temporal variations in the growth of phytoplankton cultured in ballast water, shipside water, and F/2 medium at 13°C and 20°C in April 2006.

Phytoplankton viability in ballast water from international commercial ships berthed at ports in Korea

[Table 1]
Details of the ballast tanks of ships surveyed at Ulsan and Onsan ports.

Destination(port)	Name of vessel	Tonnage (GRT)	Kind of Ship	Ballasting date	Duration time (day)	Ballasting site and Source port
Ulsan	Kinna	3,901	LPG Carrier	12th January 2006	6	Tianjin, China
Onsan	Chemstar Venus	11,951	Chemical tanker	27th December 2005	23	12 miles away Portland 46.58°N, 125.13°W
Ulsan	Eastern Goodwill	5,372	Oil/Chemical tanker	13th January 2006	6	Hongkong port
Onsan	Chemstar Belle	11,568	Oil Tanker	16th January 2006	4	Shimizu port (Japan)
Onsan	Northern Dawn	28,822	Oil Carrier	16th March 2006	20	Los Angeles, USA
Ulsan	Ikan Juara	19,885	Log & Bulk Carrier	26th and 29th March 2006	7	34-40.7 °N, 124-129 °E (Half ballast)
						Zhenjiang, China (Full ballast)

[Table 2]
Temperature, salinity, and nutrients in shipside water and ballast water of ships berthed at Ulsan and Onsan ports.

Ship name	Waters	Temperature (˚C)	Salinity (PSU)	Nutrients (μ M)	
				Nitrate	Phosphate
Kinna	S	13.0	34.0	8.9	1.1
	B	13.4	32.1	19.6	0.1
Chemstar Venus	S	9.0	34.0	10.6	1.0
	B	14.8	32.4	5.6	0.2
Eastern Goodwill	S	9.0	32.0	30.6	9.3
	B	14.7	32.6	7.5	0.5
Chemstar Belle	S	10.0	34.0	25.1	1.2
	B	12.9	33.4	5.9	0.3
Ikan Juara	S	13.0	34.0	10.6	2.2
	B	15.3	18.2	37.7	0.3
Northern Dawn	S	15.0	33.0	10.7	0.5
	B	10.6	33.3	18.1	1.3

S: shipside water, B: ballast water

[Table 3]
Initial numbers of species and concentration of dominant species among phytoplankton collected from ships' ballast tank waters for the incubation experiment.

Inoculated phytoplankton	Taxonomical groups	Kinna		Chemstar Venus		Eastern Goodwill		Chemstar Belle		Ikan Juara		Northern Dawn	
		20°C	13°C	20°C	13°C	20°C	13°C	20°C	13°C	20°C	13°C	20°C	13°C
Species number	Diatoms	3	4	1		17	18	7	9	6	4	9	8
	Dinoflagellates					1	1		1		2		
	Cryptomonads	1	1		2								
	Euglenoids	1											
	Others			2		3	2	1				2	
	Total	**5**	**5**	**3**	**2**	**21**	**21**	**8**	**10**	**6**	**6**	**11**	**8**
Concentration (cells/mL)	Dominant species	8	4	1	2	270	343	48	35	15	7	159	155
	Co-dominant species	2	3			75	101	16	7	4	3	16	4
	Total	**13**	**10**	**3**	**2**	**519**	**582**	**76**	**53**	**26**	**16**	**188**	**171**

[Table 4]
Temporal variations among dominant species during the growth period of inoculated phytoplankton in ballast water, shipside water, and F/2 medium during incubation.

Ship name	Phase	Media for incubation		
		Shipside water	Ballast water	F/2 medium
Kinna	Initial	*Cylindrotheca closterium* (A) *Cryptomonas* sp.(O, A)	*Cylindrotheca closterium* (A) *Cryptomonas* sp.(O, A)	*Cylindrotheca closterium* (A) *Cryptomonas* sp.(O, A)
	Exponential	*Thalassiosira rotula* (O, A) *Cylindrotheca closterium* (O, A) *Skeletonema costatum* (O, A) Pennate diatoms (<10㎛) (O, A)	Not observed	*Cylindrotheca closterium* (O, A) Pennate diatoms (<10㎛) (O, A)
	Last	*Thalassiosira rotula* (A) *Cylindrotheca closterium* (O) Pennate diatoms (<10㎛) (O,A)	Pennate diatoms (<10㎛) (O, A)	*Cylindrotheca closterium* (O, A) Pennate diatoms (<10㎛) (O)
Chemstar Venus	Initial	*Cylindrotheca closterium* (O) *Cryptomonas* sp.(A)	*Chaetoceros convolutus* (O) *Cryptomonas* sp.(A)	*Chaetoceros convolutus* (O) *Cryptomonas* sp.(A)
	Exponential	Pennate diatoms (<10㎛) (O) Centric diatoms (<10㎛) (O)	Pennate diatoms (<10㎛) (O) Centric diatoms (<10㎛) (O)	Pennate diatoms (<10㎛) (O) Centric diatoms (<10㎛) (O)
	Last	Pennate diatoms (<10㎛) (O) Centric diatoms (<10㎛) (O)	Pennate diatoms (<10㎛) (O, A) Centric diatoms (<10㎛) (O, A)	Pennate diatoms (<10㎛) (O, A) Centric diatoms (<10㎛) (O, A)
Eastern Goodwill	Initial	*Skeletonema costatum* (O, A) *Chaetoceros debilis* (O, A)	*Skeletonema costatum* (O, A) *Chaetoceros debilis* (O, A)	*Skeletonema costatum* (O, A) *Chaetoceros debilis* (O, A)
	Exponential	*Lauderia annulata* (O) *Skeletonema costatum* (O) *Cylindrotheca closterium* (O)	Not observed	*Lauderia annulata* (O) *Skeletonema costatum* (O, A) *Cylindrotheca closterium* (O) Pennate diatoms (<10㎛) (O)
	Last	Pennate diatoms (<10㎛) (O,A)	Not observed	*Cylindrotheca closterium* (O) Pennate diatoms (<10㎛) (O, A)
Chemstar Belle	Initial	*Eucampia zodiacus* (O, A) *Chaetoceros debilis* (O, A)	*Eucampia zodiacus* (O, A) *Chaetoceros debilis* (O, A)	*Eucampia zodiacus* (O, A) *Chaetoceros debilis* (O, A)
	Exponential	*Chaetoceros debilis* (O, A) *Stephanophyxis turris* (O, A) *Nitzschia longissima* (O, A) *Skeletonema costatum* (A) Pennate diatoms (<10㎛) (O,A)	Pennate diatoms (<10㎛) (O, A) *Cylindrotheca closterium* (A)	*Cylindrotheca closterium* (O,A) Pennate diatoms (<10㎛) (O, A)
	Last	Pennate diatoms (<10㎛) (O) *Skeletonema costatum* (A)	Pennate diatoms (<10㎛) (O)	*Cylindrotheca closterium* (O, A) Pennate diatoms (<10㎛) (O, A)
Ikan Juara	Initial	*Nitzschia* sp.(O, A) *Asterionella formosa* (A) *Lauderia annulata* (O)	*Nitzschia* sp. (O, A) *Asterionella formosa* (A) *Lauderia annulata* (O)	*Nitzschia* sp. (O, A) *Asterionella formosa* (A) *Lauderia annulata* (O)
	Exponential	Pennate diatoms (<10㎛) (O, A)	*Detonula* sp. (O, A) Pennate diatoms (<10㎛) (O,A)	*Detonula* sp. (O, A) Pennate diatoms (<10㎛) (O, A)
	Last	*Detonula* sp. (O, A) Pennate diatoms (<10㎛) (O,A)	*Detonula* sp. (O) Pennate diatoms (<10㎛) (O, A)	Pennate diatoms (<10㎛) (O,A)
Northern Dawn	Initial	*Skeletonema costatum* (O, A) *Nitzschia* sp.(O) *Thalassiosira* sp.(A)	*Skeletonema costatum* (O, A) *Nitzschia* sp.(O) *Thalassiosira* sp.(A)	*Skeletonema costatum* (O, A) *Nitzschia* sp.(O) *Thalassiosira* sp.(A)
	Exponential	*Skeletonema costatum* (O, A) *Cylindrotheca closterium* (O)	*Skeletonema costatum* (O, A)	*Skeletonema costatum* (O, A)
	Last	*Skeletonema costatum* (O, A) *Cylindrotheca closterium* (O)	*Skeletonema costatum* (O)	*Skeletonema costatum* (O, A)

O: optimal temperature (20°C), A: ambient temperature (13°C)

An integrated translation of design data of a nuclear power plant from a specification-driven plant design system to neutral model data

Mun, D.
Marine Safety & Pollution Response Research Department
•
dhmun@moeri.re.kr

How to efficiently integrate and manage lifecycle data of a nuclear power plant has gradually become an important object of study. Because plants usually have a very long period of operation and maintenance, the plant design data need to be presented in a computer-interpretable form and to be independent of any commercial systems. The conversion of plant design data from various design systems into neutral model data is therefore an important technology for the effective operation and maintenance of plants. In this study, a neutral model for the efficient integration of plant design data is chosen from among the currently available options and extended in order to cover the information model requirements of nuclear power plants in Korea. After the mapping of the neutral model and the data model of a specification-driven plant design system, a plant data translator is also implemented in accordance with the schema mapping results.

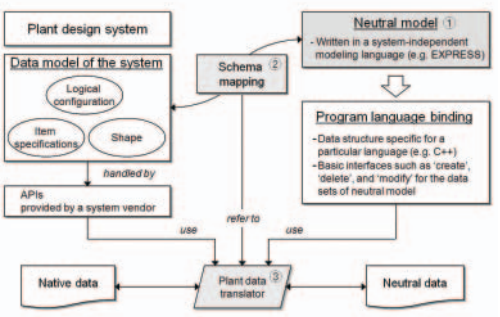

[Figure 1]
Translation process of the plant design data

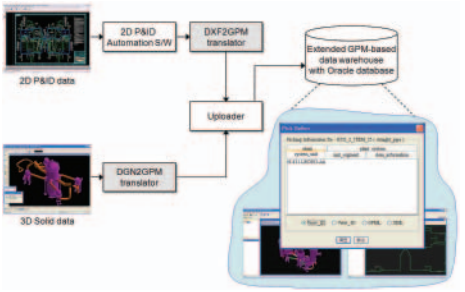

[Figure 2]
Integrated translation of plant design data into the extended GPM data.

Complete Genome Sequence of *"Candidatus Puniceispirillum marinum"* IMCC1322, a representative of the SAR116 clade in the Alphaproteobacteria

Hong Gun Sung
Marine Structure & Plant Research Department
●
hgsung@moeri.re.kr

One of the major uncultured ubiquitous marine bacteria clade SAR116 in the Alphaproteobacteria had been reported after investigation of Giovannoni et al. in 1990. This group comprises 5~10% of total bacteria at surface layer of ocean, however, the physiological and genetic characteristics has been not known due to the rack of isolates. The strain IMCC1322 was the first cultivate of the SAR116 clade that isolated from the East Sea, Korea by research group of Inha University. After that KORDI and Inha Univ. has been cowork to understand the physiology and ecology of the strain and at first report the complete genome sequence of "Candidatus Puniceispirillum marinum" IMCC1322. The genome contained genes for proteorhodopsin, aerobic-type carbon monoxide dehydrogenase, dimethylsulfoniopropionate demethylase, and C1 compound metabolism. The genome information proposes the SAR116 group as metabolic generalists carrying functional genes for utilizing resourceful sunlight, DMSP, CO, and C1 compounds in the surface ocean. Such metabolic potential of strain IMCC1322 might be epitomizing ecological niches for even more dominant marine bacterioplankton clades SAR11, Roseobacter, and SAR86.

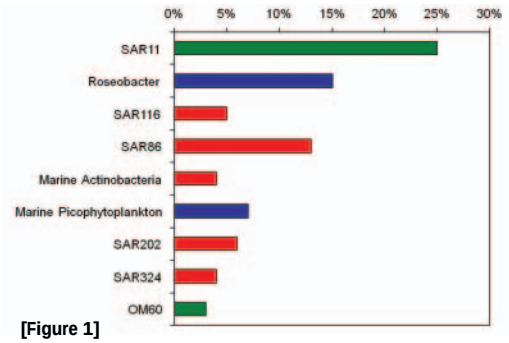

[Figure 1]
Proportion and status of dominant marine bacteria in the surface layer.
Blue : Cultivated and identified validly, Green : Cultivated in recently but not validly identified. Red : No cultivated has been reported

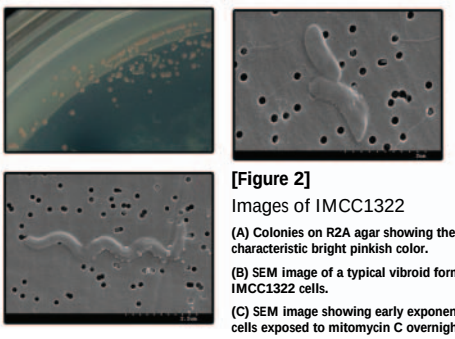

[Figure 2]
Images of IMCC1322
(A) Colonies on R2A agar showing the characteristic bright pinkish color.
(B) SEM image of a typical vibroid forms of IMCC1322 cells.
(C) SEM image showing early exponential-phase cells exposed to mitomycin C overnight.

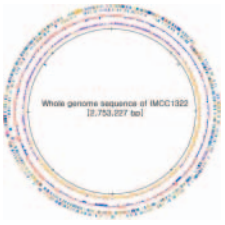

[Figure 3]
Whole genome sequence of strain IMCC1322.

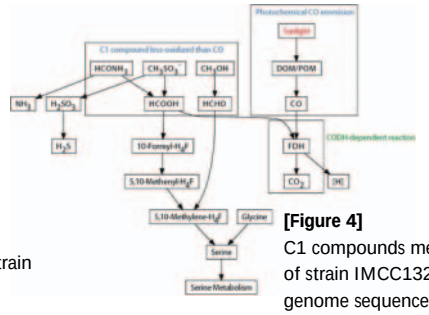

[Figure 4]
C1 compounds metabolic pathway of strain IMCC1322 deduced from genome sequence.

Hebei Spirit oil spill monitored on site by fluorometric detection of residual oil in coastal waters off Taean, Korea

Kim, Moon koo
South Sea Environment Research Department
•
mkim@kordi.re.kr

The spatiotemporal distributions of dissolved and/or dispersed oil in seawater and pore water were monitored on site by fluorometric detection method after the Hebei Spirit oil spill. The oil concentrations in intertidal seawater, 15 days after the spill, were as high as 16,600 ?g/L and appeared to decrease below the Korean marine water quality standard of 10 ?g/L at most sites 10 months after the spill. Fluorometric detection of oil in pore water was introduced to eliminate the effects of grain size for the quantification of oil in sediments and to better explain spatial and temporal distribution of oil pollution at sandy beaches. The fluorescence detection method was compared with the conventional laboratory technique of total petroleum hydrocarbon analysis using gas chromatography. The method of fluorescence detection of oil was capable of generating results much faster and more cost-effectively than the traditional GC technique.

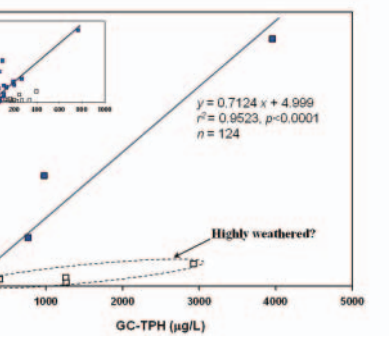

[Figure 3]
Comparison of two quantification methods of oil (fluorometric vs. gas chromatographic). GC-TPH represents oil concentrations determined by conventional gas chromatographic method; fluorescence-TPH represents oil concentrations measured by on-site fluorometric method. Supposedly highly weathered samples (high GC-TPH content but low fluorescence) are marked with open square (□) and excluded from linear regression analysis (y=0.7124x+4.999, r^2=0.9523, p<0.0001, n=124). The inset figure shows the smaller scale concentration range of the data for the main figure.

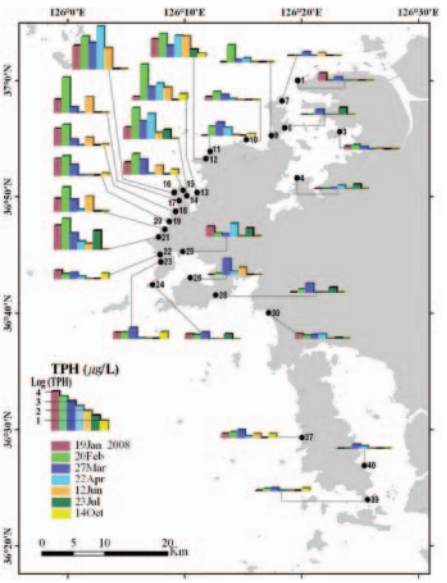

[Figure 1]
Spatiotemporal distributions of oil contaminations in seawater monitored on site using fluorescence detector. Oil concentrations in seawater are expressed as log (total petroleum hydrocarbons) (μg/L).

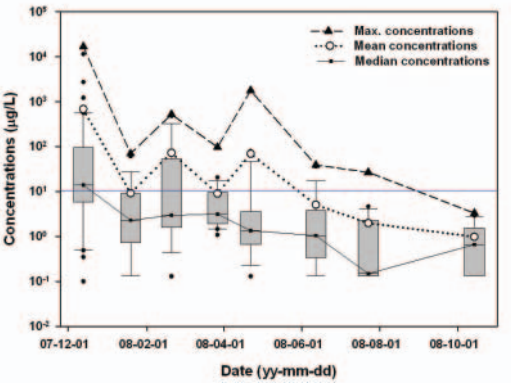

[Figure 2]
Box-and-whiskers plots showing temporal variations of residual oil in seawater monitored from Dec. 13, 2007 through Oct. 14, 2008 using portable fluorescence detector at the oil spill site, Taean, Korea. The bottom and top of the grey box indicate the 25th and 75th percentile of the data and the ends of the whiskers represent the 10th and 90th percentile. Note that oil concentrations are in a logarithmic scale and the horizontal line at 10 μg/L indicates the marine water quality threshold in Korea.

Warm Pool and Cold Tongue El Niño events as simulated by the GFDL 2.1 coupled GCM

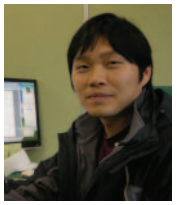

Kug, Jong Seong
Climate Change & Coastal Disaster Research Department
•
jskug@kordi.re.kr

Recent studies report that two types of El Niño events have been observed. One is the cold tongue (CT) El Niño, which is characterized by relatively large sea surface temperature (SST) anomalies in the eastern Pacific, and the other is warm pool (WP) El Niño, in which SST anomalies are confined to the central Pacific. In this study, we analyze both types of El Ni?o events in a long-term coupled GCM simulation. The present model simulates the major observed features of both types of El Niño, incorporating the distinctive patterns of each oceanic and atmospheric variable. It is also demonstrated that each type of El Niño has quite distinct dynamic processes, which control their evolutions. The CT El Niño exhibits strong equatorial heat discharge to the poleward and thus the dynamical feedbacks control the phase transition from a warm event to a cold event. On the other hand, the discharge process in the WP El Niño is weak due to its spatial distribution of ocean dynamic field. The positive SST anomaly of WP El Ni?o is thermally damped through the intensified evaporative cooling

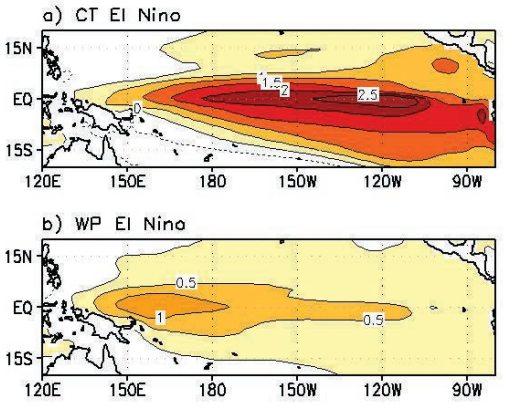

[Figure 1]
SST anomaly (℃) composite of the (a) CT El Niño and (b) WP El Niño during ND(0)JJ(1).

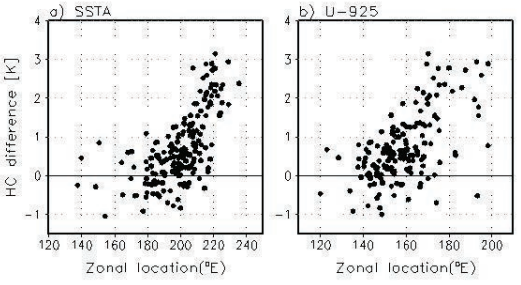

[Figure 2]
Scatter plots between the discharge of the heat content and the zonal location of the (a) SST anomaly and the (b) zonal wind at 925-hPa.